

Magnetic and charge orders on the triangular lattice: Extended Hubbard model with intersite Ising-like magnetic interactions in the atomic limit

Konrad Jerzy Kacpia^a, Jan Barański^b

^a*Institute of Spintronics and Quantum Information, Faculty of Physics, Adam Mickiewicz University in Poznań, ul. Uniwersytetu Poznańskiego 2, 61614 Poznań, Poland*

^b*Department of General Education, Polish Air Force University, ul. Dywizjonu 303 nr 35, 08521 Deblin, Poland*

ARTICLE INFO

Keywords:

charge order and metamagnetism
metastable phases
triangular lattice
fermionic lattice gas
extended Hubbard model
atomic limit

ABSTRACT

In the work, we investigated a generalized model of the fermionic lattice gas in the form of the extended Hubbard model with intersite Ising-like interactions (both antiferromagnetic and ferromagnetic) at the atomic limit on the triangular lattice. In the ground state, we find the exact phase diagram as a function of μ . Within the mean-field decoupling of the intersite term and exact treatment of onsite interaction, we found also the diagrams for $T \geq 0$ including metastable phases. For antiferromagnetic coupling, we find that nontrivial ordered phase can exist with coexistence of charge and metamagnetic ordering. The transition between the ordered phase and the nonordered phase can be discontinuous as well continuous depending on the model parameters. Moreover, the ordered phase can coexist with the nonordered phase in phase separated states for fixed electron concentration. Additionally, the ranges of phases metastability are determined in the neighborhood of the discontinuous transitions.

HIGHLIGHTS:

- The extended Hubbard model with intersite Ising-like interactions is investigated.
- Orderings on the triangular lattice with geometrical frustration are analyzed.
- The exact ground state for fixed chemical potential is determined.
- Mean-field solutions of the model for finite temperatures are found and discussed.
- Complex phase diagram for both signs of magnetic interactions are determined.

1. Introduction

The strongly correlated system exhibits many intriguing phenomena from band renormalization to very complex diagrams with phases involving charge, spin, orbital or superconducting orders [1–4]. Moreover, the ability of controlling the interactions in the ultra-cold fermionic gases on the optical lattices via Feshbach resonances releases the new possibilities for experimental studies of variety of unconventional systems [5, 6], in particular, in systems with geometrical frustration [7, 8].

Inspired by the rich structure of the simple model of charged ordered insulators on the triangular lattice [9–11], in this work, we investigate a generalized model of the strongly correlated fermionic lattice gas, which can be also considered as a generalization of the standard $S = 1/2$ Ising model [12–18]. The studied Hamiltonian has the following form [19–26]:

$$\hat{H} = U \sum_i \hat{n}_{i,\uparrow} \hat{n}_{i,\downarrow} + 2J \sum_{\langle i,j \rangle} \hat{s}_i \hat{s}_j - \mu \sum_i \hat{n}_i, \quad (1)$$

where $\hat{n}_{i,\sigma} = \hat{c}_{i,\sigma}^\dagger \hat{c}_{i,\sigma}$, $\hat{s}_i = \frac{1}{2} (\hat{n}_{i,\uparrow} - \hat{n}_{i,\downarrow})$, and $\hat{c}_{i,\sigma}^\dagger$ ($\hat{c}_{i,\sigma}$) denotes the creation (annihilation) operator of a fermion with spin σ ($\sigma \in \{\uparrow, \downarrow\}$) at lattice site i . U is onsite Hubbard interaction, J is intersite Ising-like magnetic interaction

between nearest-neighbor sites i and j , and μ denotes the chemical potential. $\sum_{\langle i,j \rangle}$ indicates summation over nearest-neighbor sites independently. Note that, for $U \rightarrow +\infty$ and $n = 1$ (or $\mu = U/2$; the half-filling), model (1) reduces to the Ising model (with two possible states $s_i = \pm 1/2$ on a single lattice site) in the absence of the external field (in a general case, in the external field of $\mu - U/2$).

The model has been intensively analyzed on the alternate (bipartite) lattices. The case of one-dimensional chain without and with the external magnetic field was investigated in [21, 27] and [22], respectively. Classical Monte Carlo simulations were performed for the model on two-dimensional square lattice system [20, 23–25]. Finally, rigorous results (in the limit of $d \rightarrow +\infty$) for model (1) considered on the hypercubic lattices were obtained in [19, 25, 28, 29] with the use of the variational approach with the mean-field approximation for the intersite term and a rigorous treatment of the local interactions.

The investigated model exhibits the particle-hole symmetry, thus, it is enough to analyze the model for $\mu < U/2$ (or $n < 1$). Note that for the model on the hypercubic lattices, the $J \leftrightarrow -J$ symmetry occurs [25], but for the triangular lattice it is no longer valid.

2. Mean-field expressions for finite temperatures

The method based on the mean-field approximation for the intersite terms (where as the onsite terms treated exactly)

✉ konrad.kacpia@amu.edu.pl (K.J. Kacpia); j.baranski@law.mil.pl

(J. Barański)

ORCID(s): 0000-0001-8842-1886 (K.J. Kacpia); 0000-0002-0963-497X (J. Barański)

is applied for model (1) to find thermodynamic behavior of the model at arbitrary temperatures (details of the method can be found in, e.g., [10, 25, 30]). The grand canonical potential is determined as

$$\omega = -\frac{1}{3} \sum_{\alpha} \psi_{\alpha} s_{\alpha} - \frac{1}{3\beta} \sum_{\alpha} \ln Z_{\alpha}, \quad (2)$$

where $\beta = 1/(k_B T)$ is inverted temperature (k_B is the Boltzmann constant), coefficients ψ_{α} for $\alpha \in \{A, B, C\}$ are defined as $\psi_A = J(s_B + s_C)$, $\psi_B = J(s_A + s_C)$, $\psi_C = J(s_A + s_B)$, and

$$Z_{\alpha} = 1 + \exp[\beta(2\mu - U)] + 2 \exp(\beta\mu) \cosh(\beta\psi_{\alpha}). \quad (3)$$

Equations for concentrations $n_{\alpha} = \langle \hat{n}_i \rangle_{i \in \alpha}$ and magnetizations $s_{\alpha} = \langle \hat{s}_i \rangle_{i \in \alpha}$ in each sublattice $\alpha \in \{A, B, C\}$ are obtained as

$$n_{\alpha} = \frac{2}{Z_{\alpha}} \left\{ \exp[\beta(2\mu - U)] + \exp(\beta\mu) \cosh(\beta\psi_{\alpha}) \right\}, \quad (4)$$

$$s_{\alpha} = \frac{1}{Z_{\alpha}} \exp(\beta\mu) \sinh(-\beta\psi_{\alpha}). \quad (5)$$

One can also derive expressions for other quantities, e.g., for double occupancy $D_{\alpha} = \langle \hat{n}_{i,\uparrow} \hat{n}_{i,\downarrow} \rangle_{i \in \alpha}$ and for local magnetic moment $\gamma_{\alpha} = \langle |\hat{s}_i| \rangle_{i \in \alpha}$ as

$$D_{\alpha} = \frac{1}{Z_{\alpha}} \exp(2\mu - U), \quad \gamma_{\alpha} = \frac{1}{Z_{\alpha}} \exp(\beta\mu) \cosh(\beta\psi_{\alpha}).$$

These quantities are related by $D_{\alpha} + \gamma_{\alpha} = n_{\alpha}/2$. They also determine the fraction of single and double occupied sites, respectively, in each sublattice. $2D_{\alpha}$ and $2\gamma_{\alpha}$ stand for the numbers of locally paired and unpaired particles, respectively, in each sublattice. The total particle concentration n is defined as $n = \sum_{\alpha} n_{\alpha}/3$.

Note that the right hand side of Eq. (4) [as well as Eq. (3)] does not include n_{α} 's. Thus, effectively one needs to solve self-consistently a set of only three non-linear equations (5) to determine s_A , s_B , and s_C (for fixed model parameters $\mathcal{P} = \{\mu, U, J, T\}$). n_{α} 's are determined by s_{α} 's and parameters \mathcal{P} . However, the set can have several solutions for s_{α} and one needs to find the solution corresponding to the lowest ω determined by (2). Due to the symmetry of the system, there are several solutions, which are equivalent with (s_A, s_B, s_C) solution, e.g., $(-s_A, -s_B, -s_C)$, (s_B, s_C, s_A) , (s_C, s_A, s_B) , (s_B, s_A, s_C) . In total, there can be 12 equivalent solutions, but their number is reduced if there are some particular relations between s_{α} 's, e.g., if $s_A = -s_B$.

From numerical analysis of equations (5) for antiferromagnetic interactions ($J > 0$) presented in Sec. 4, one gets that the solutions, which correspond to the lowest ω , have the form of $(s, -s, 0)$ (there is 6 such equivalent solutions). If $|s| > 0$, we call this phase the AFT phase (antiferromagnetic alignment of average magnetic moments in two sublattices, in the third one - no magnetization), whereas, if $s = 0$, it is the normal (non-ordered, NO) phase. Note that, if, e.g., $s_A = -s_B$ for some \mathcal{P} , one gets immediately that $\psi_C = 0$

and, from (5), $s_C = 0$ for that \mathcal{P} . In such case, Eqs. (5) and (2) take the forms

$$s = \frac{\sinh(\beta J s)}{2 [\cosh(\beta \bar{\mu}) \exp(-\beta U/2) + \cosh(\beta J s)]}, \quad (6)$$

$$\omega = -\bar{\mu} - \frac{2}{3} J s - \frac{1}{3\beta} \ln [2 \cosh(\beta \bar{\mu}) + 2 \exp(\beta U/2)] - \frac{2}{3\beta} \ln [2 \cosh(\beta \bar{\mu}) + 2 \exp(\beta U/2) \cosh(\beta J s)]. \quad (7)$$

In the case of the ferromagnetic coupling ($J < 0$), the lowest ω solutions are found as (s, s, s) (two equivalent solutions), and the only ordered phase occurring is the ferromagnetic (FER) phase (for $|s| > 0$). In such a case, equations (4)–(5) reduce to those obtained in Ref. [25]. Then, Eqs. (5) and (2) take the forms

$$s = \frac{\sinh(-\beta 2 J s)}{2 [\cosh(\beta \bar{\mu}) \exp(-\beta U/2) + \cosh(\beta 2 J s)]}, \quad (8)$$

$$\omega = -\bar{\mu} - 2 J s - \frac{1}{\beta} \ln [2 \cosh(\beta \bar{\mu}) + 2 \exp(\beta U/2) \cosh(\beta 2 J s)]. \quad (9)$$

Thus, for the ferromagnetic coupling J within the mean-field approximation, the results for model (1) on the triangular lattice and on the bipartite lattices are the same (cf. also Refs. [19, 20]). Note that, for the model on the alternate lattices (in the absence of the external magnetic field, analyzed in detail in Refs. [19, 20, 25]), the sign of the nearest-neighbor magnetic coupling is irrelevant for the phase boundaries and only type of order in the ordered phase is different: if $J < 0$ the ferromagnetic order exists, whereas for $J > 0$ the antiferromagnetic order appears.

One can notice that Eqs. (6) and (8) (variables with AFT and FER labels, respectively) give the same solution for s ($s_{\text{FER}} = s_{\text{AFT}}$) if $J_{\text{AFT}} = -J_{\text{FER}} > 0$ and

$$T_{\text{AFT}} = \frac{T_{\text{FER}}}{2}, \quad \bar{\mu}_{\text{AFT}} = \frac{\bar{\mu}_{\text{FER}}}{2}, \quad U_{\text{AFT}} = \frac{U_{\text{FER}}}{2} \quad (10)$$

and $\beta_{\text{AFT}} = 2\beta_{\text{FER}}$. The relation between concentration in both ordered phases can be obtained from Eq. (4) with using (10) and one gets

$$2n_{\text{FER}}(T_{\text{FER}}, U_{\text{FER}}, \bar{\mu}_{\text{FER}}) = 3n_{\text{AFT}}(T_{\text{AFT}}, U_{\text{AFT}}, \bar{\mu}_{\text{AFT}}) - n_{\text{NO}}, \quad (11)$$

where n_{NO} is the total concentration in the non-ordered phase and $n_{\text{NO}}(T_{\text{FER}}, U_{\text{FER}}, \bar{\mu}_{\text{FER}}) = n_{\text{NO}}(T_{\text{AFT}}, U_{\text{AFT}}, \bar{\mu}_{\text{AFT}})$. Note also that conditions for the order-disorder boundaries, i.e., $\omega_{\text{NO}} = \omega_{\text{AFT}}$ and $\omega_{\text{NO}} = \omega_{\text{FER}}$ (where ω_{NO} denotes ω for $s = 0$) also can be transformed into each other using (10). Because of that, in the following, we will focus mainly on model (1) with antiferromagnetic interactions (i.e., $J > 0$).

Note that both Eqs. (6) and (8) can be rewritten as

$$s = \frac{\sinh(\beta k J s)}{2 [\cosh(\beta \bar{\mu}) \exp(-\beta U/2) + \cosh(\beta k J s)]}, \quad (12)$$

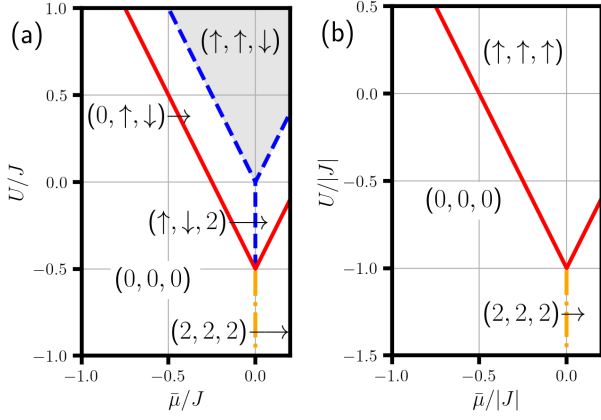


Figure 1: Ground state phase diagram of the model for (a) $J > 0$ and (b) $J < 0$ (as a function of $\bar{\mu} = \mu - U/2$, rigorous results). The regions are labeled by configuration in the elementary block (defined in text). Different lines denote the boundaries with infinite (macroscopic) degeneracy [dashed (blue) line] and finite degeneracy [solid (red) and dot-dashed (orange) lines]. Dot-dashed (orange) lines denotes the boundaries which vanishes at any infinitesimally small $T > 0$ (within the MFA). Grey shadow denotes a region with infinite degeneracy. The regions are labeled by the arrangement in the elementary block.

where (i) $k = 1$ if $J > 0$ (the AFT phase) or (ii) $k = -2$ if $J < 0$ (the FER phase). Using similar procedure as in [10, 11, 29, 30], taking the limit of $s \rightarrow 0$ of both sides of the equation above (divided by s before) and applying the de l'Hospital theorem) one gets the expression for the second order temperature T_c for order-disorder transition as

$$k_B T_c / J = (kt) (1 + 2t + t^2 a)^{(-1)}, \quad (13)$$

where $t = \exp(\beta_c \mu)$, $a = \exp(-\beta_c U)$, $\beta_c = 1/(k_B T_c)$. At the boundary the relation between μ and n is expressed by $\mu = (1/\beta_c) \ln(x)$, where $x = (n - 1 + \sqrt{y}) / ((2 - n)a)$ and $y = (1 - n)^2 + n(2 - n)a$. All found continuous boundaries on the diagrams presented in Sec. 4 fulfill condition (13). Moreover, the solutions of (13) coincide with the metastability boundaries for the NO phase.

3. The ground state results

To determine the ground state phase diagram as a function of the chemical potential the elementary block method is used, which is described in detail in Refs. [10, 31–36]. In these works, it was used for the atomic limit of the extended Hubbard model with intersite density-density interactions, but it can be also applied to model (1) to determine the grand canonical potential ω_0 (per site) at $T = 0$. In the model, at each site the following four states are possible: 0 (empty), \uparrow (particle with spin-up), \downarrow (particle with spin-down), 2 (double occupied), which characterize the elementary block. The total number of them is $3^4 = 81$, but some of them are equivalent due to spin-inversion symmetry of the model

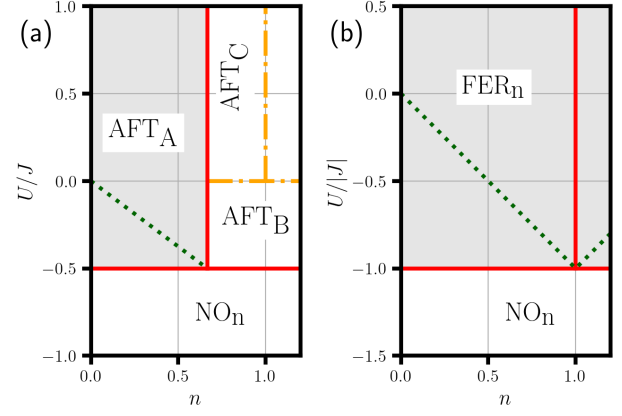


Figure 2: Ground state phase diagram of the model for (a) $J > 0$ and (b) $J < 0$ (as a function of n). The regions are labeled by homogeneous phases (defined in text). Shadows denote regions, where phase separated states have lower energy (at $T \geq 0$). The dotted line denotes the boundary between homogeneous phases in the region of the PS state occurrence. Dot-dashed (orange) lines denotes the boundaries, which vanishes at any infinitesimally small $T > 0$.

and permutation of the sublattice labels (e.g., $(0, \uparrow, \downarrow)$ is equivalent with $(\downarrow, \uparrow, 0)$).

The resulting ground state phase diagrams of the model (1) for both signs of J interaction are presented in Fig. 1. The following arrangements appear in Fig. 1(a) (for $J > 0$): $(0, 0, 0)$ with $\omega_0 = 0$; $(0, \uparrow, \downarrow)$ with $\omega_0 = -J/6 - 2\mu/3$; $(\uparrow, \uparrow, \downarrow)$ with $\omega_0 = -J/6 - \mu$; $(2, \uparrow, \downarrow)$ with $\omega_0 = U/3 - J/6 - 4\mu/3$; and $(2, 2, 2)$ with $\omega_0 = U - 2\mu$. Note that block $(\uparrow, \uparrow, \downarrow)$ appearing in Fig. 1(a) is equivalent to $(\downarrow, \uparrow, \downarrow)$ and $(\uparrow, \downarrow, \downarrow)$. Therefore, inside its region, at least two of those three equivalent configurations can be mixed freely. Consequently, in the shadowed region, the ground state is infinitely degenerated (and the entropy per site is nonzero). Similarly, at the dashed boundaries, blocks from neighboring regions can mix with each other freely, e.g., $(0, \uparrow, \downarrow)$ with $(\uparrow, \uparrow, \downarrow)$ (coexistence at the microscopic level). In the mean-field approximation, in this region, a phase with $s_C = 0$ occurs. For $J < 0$ (Fig. 1(b)), apart from $(0, 0, 0)$, and $(2, 2, 2)$, the region of $(\uparrow, \uparrow, \uparrow)$ with $\omega_0 = J/2 - \mu$ is present. This is in agreement with [19, 25].

To find the phase diagram at $T = 0$ as a function of total particle concentration $n = (n_A + n_B + n_C)/3$, we determine the ground state free energies $f_0 = \omega_0 + \mu n$ for the homogeneous phases in the mean-field approximation (cf. also [10, 36]). We use the following denotations for phase properties: $\vec{N} \equiv (n_A, n_B, n_C)$ (describing charge ordering), $\vec{S} \equiv (s_A, s_B, s_C)$ (describing spin ordering), $\vec{D} \equiv (D_A, D_B, D_C)$ (double occupancies).

One gets the following results for appearing homogeneous phases: (i) nonordered NO_n with $\vec{N} = (n, n, n)$, $\vec{S} = (0, 0, 0)$, $\vec{D} = (n/2, n/2, n/2)$ and $f_0 = Un/2$; three AFT phases (distinguishable only at $T = 0$): (ii) AFT_A with $\vec{N} = (0, 3n/2, 3n/2)$, $\vec{S} = (0, 3n/4, -3n/4)$, $\vec{D} = (0, 0, 0)$ and $f_0 = -3Jn^2/8$; (iii) AFT_B with $\vec{N} = (3n - 2, 1, 1)$,

$\vec{S} = (0, 1/2, -1/2)$, $\vec{D} = ((3n - 2)/2, 0, 0)$ and $f_0 = U(3n - 2)/6 - J/6$; (iv) AFT_C with $\vec{N} = (3n - 2, 1, 1)$, $\vec{S} = (0, 1/2, -1/2)$, $\vec{D} = (0, 0, 0)$ and $f_0 = -J/6$; and (v) ferromagnetic FER_n with $\vec{N} = (n, n, n)$, $\vec{S} = (n/2, n/2, n/2)$, $\vec{D} = (0, 0, 0)$ and $f_0 = Jn^2/2$. Apart from the AFT_A and the FER_n phases, all of them are degenerated with phase separates states in which two domains of commensurate phases (with $n = 0, 2/3, 4/3, 2$) coexist (mentioned previously for fixed μ and existing on the boundaries of regions from Fig. 2). This degeneracy is removed at finite temperatures. Note that AFT_A and the FER_n are unstable in their ranges of occurrence, i.e., $\partial^2 f / \partial n^2 < 0$. It turns out that, for $J > 0$, the PS state (with domains $(0, \uparrow, \downarrow)$ and $(0, 0, 0)$) exists (with $f_0 = -Jn/4$), whereas for $J < 0$, the PS state (with domains $(\uparrow, \uparrow, \uparrow)$ and $(0, 0, 0)$) has the lowest free energy ($f_0 = Jn/2$) in the areas depicted by shadow in Fig. 2. The dotted line denotes the boundary between homogeneous phases inside the regions of the PS state occurrence.

4. Finite temperatures phase diagrams ($J > 0$)

This section is devoted for a discussion of the phase diagrams of the model, including the metastable phases for $J > 0$. Exemplary phase diagrams as a function of chemical potential are presented in Fig. 3 (cf. also [25]). In finite temperatures, only two phases occur on the phase diagram: the NO phase and the AFT phase. For fixed $\bar{\mu}/J$ and $U/J > 0$, at temperatures above the threshold of $J/(6k_B)$, the transition between the NO and AFT phases is second order (cf. solid lines in Fig. 3(a)) and metastable phases does not appear. The transition changes its order at the tricritical point (TCP) and for temperatures below $J/(6k_B)$, the transition changes its order to the first one (dashed lines). Discontinuity of the transition allows for appearance of metastable phases, i.e., solutions with higher ω 's than those for stable solution with the lowest ω (both stable and metastable solutions need to be local minima of $\omega(s)$). Indeed, we find the regions, in which such phases emerge. These regions (in Fig. 3) are limited by dashed lines from one side and dash-dotted lines from the other. The transition temperature is always decreasing function of $|\bar{\mu}|/J$ with its maximum at $\bar{\mu} = 0$.

Upon decreasing U/J ratio, the TCP shifts towards $\bar{\mu} = 0$. Along with this effect, the boundary of metastable NO phases expands towards $\bar{\mu} = 0$ (inside the region of the AFT phase stability). For a critical value of $U = 0$, the metastable NO phase boundary reaches $\bar{\mu} = 0$ at zero temperature (result not presented) and the NO phase is metastable for any $\bar{\mu}$ at $T = 0$. The decrease of U/J below zero causes that the metastable NO phase occurs at $\bar{\mu} = 0$ (in the region of the AFT phase stability) even for non-vanishing temperatures (Fig. 3(b)). At $U/J = -1/3 \ln 2 \approx -0.23$, the second order boundary vanishes and the AFT-NO transition is discontinuous for all range of $\bar{\mu}$ and at any temperature (Fig. 3(c)). Comparing the right sides of Figs. 3(b) and 3(c) one can note that with further decreasing of U/J ratio, the AFT phase region, where metastable NO phase is not

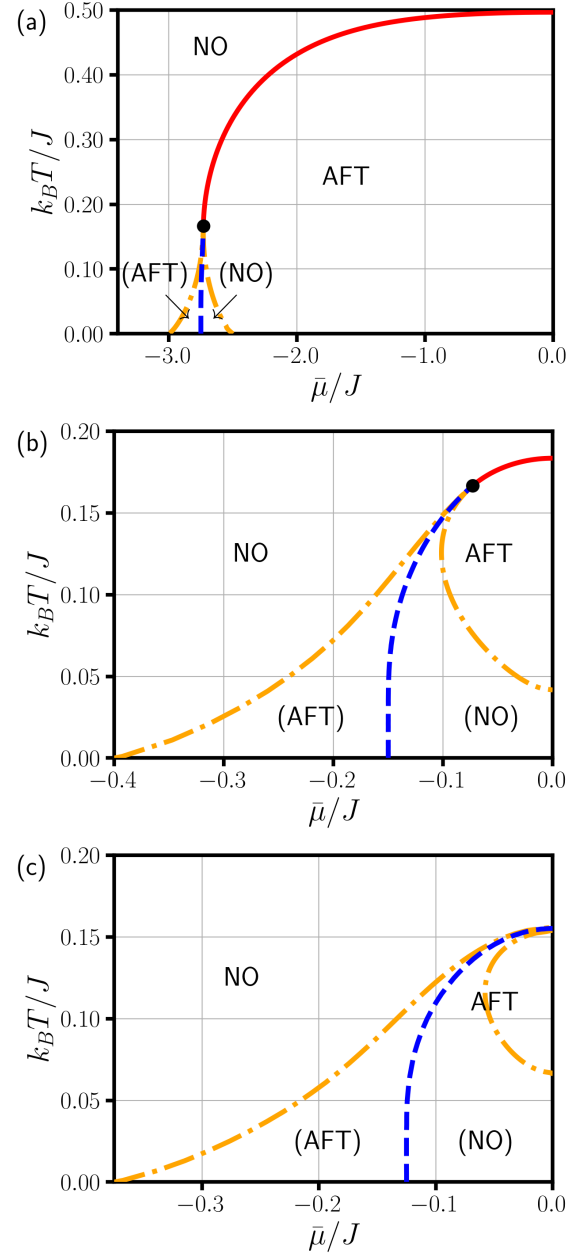


Figure 3: Phase diagrams for $U/J = 5.00$, $U/J = -0.20$, $U/J = -0.25$ as a function of $\bar{\mu} = \mu - U/2$. Solid and dashed lines denote continuous and discontinuous transitions between the AFT and NO phases, whereas dash-dotted lines indicate the boundaries of metastable phase occurrence (names of metastable phases in brackets).

present, shrinks (cf. the regions restricted by the right dash-dotted line). Below $U/J = -0.279$ this region vanishes completely and in the whole region of the AFT phase stability, the metastable NO phase occurs as well (similar effect has been predicted previously for the metastable NO phase inside superconducting phase [37]). For $U/J < -1/2$ the AFT region vanishes and only the NO phase is stable. The ordered AFT phase does not have the lowest energy for any

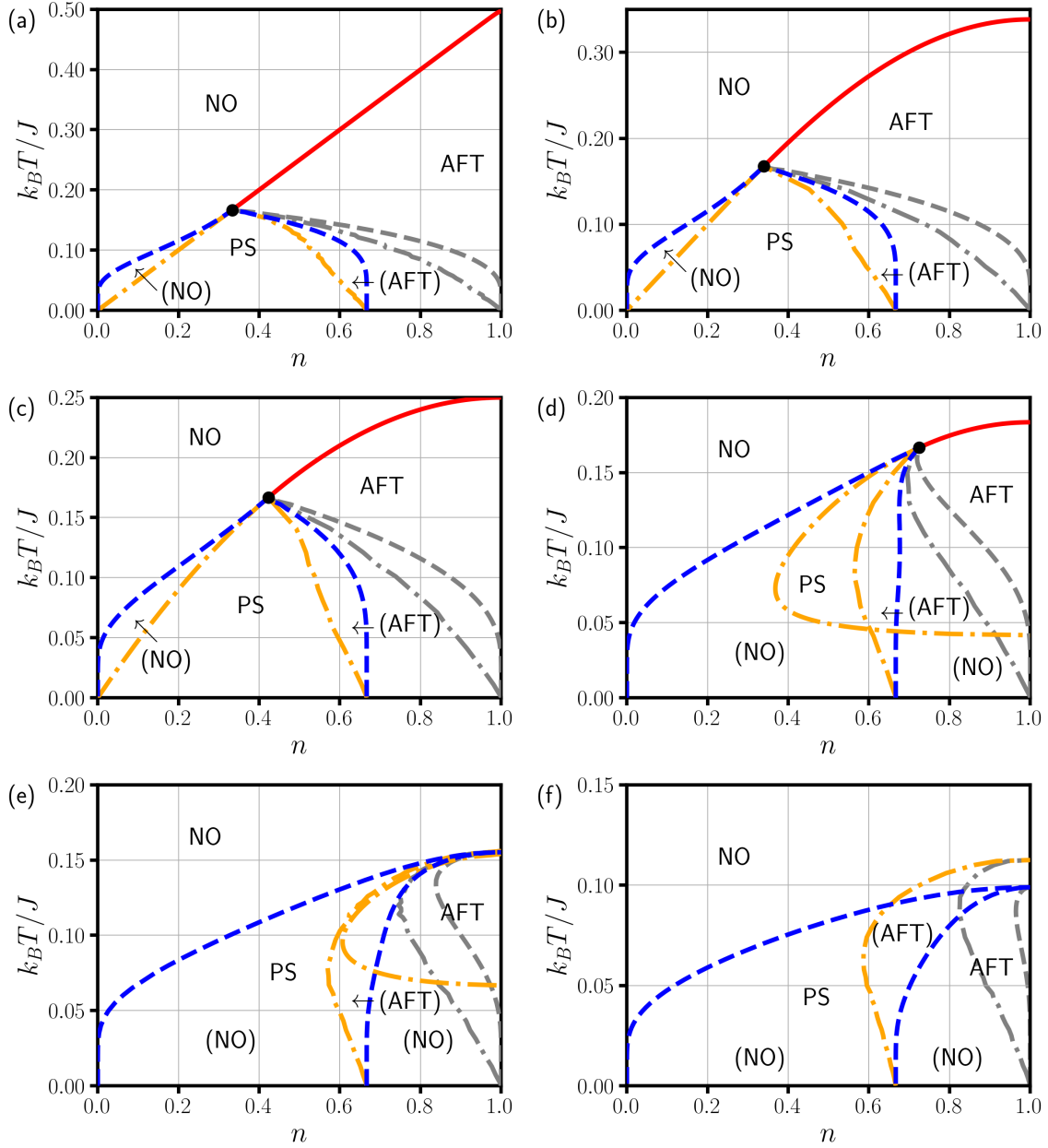


Figure 4: Phase diagrams for (a) $U/J = 5.0$, (b) $U/J = 0.5$, (c) $U/J = 0.0$, (d) $U/J = -0.2$, (e) $U/J = -0.25$, and (f) $U/J = -0.35$ ($J > 0$ AF) as a function of n . Dashed blue lines denote the boundaries for the PS state occurrence. Grey dotted line denotes line shapes for a case of $J < 0$ and the FER phase occurrence ($k_B T/|J|$ and $U/|J|$ should be multiplied by factor 2 according to Eq. (10)). Other denotations as in Fig. 3.

model parameters (is not stable), but up to $U/J = -1$, the AFT is still metastable near the half-filling ($\bar{\mu} = 0$).

The phase diagrams as a function of n are presented in Fig. 4 obtained by comparing the free energies $f = \omega + \mu n$. For $U > 0$ the diagrams are rather straightforward (cf. Fig. 4(a)-(c)). For temperatures above $k_B T = J/6$, the transition between the AFT and the NO homogeneous phases is continuous. For temperatures below this threshold, the discontinuous NO-AFT boundary (for fixed $\bar{\mu}$) splits into two lines (dashed lines in Fig. 4). Between these two (dashed) lines the phase-separated (PS) state occurs. This

state is characterized by the coexistence of two domains (of the AFT and NO phases) in the system (macroscopic phase separation). More details about such PS states and application of the Maxwell's construction for correlated system can be found, e.g., in Refs. [10, 25, 36, 38, 39]. We note that, inside the region of the PS occurrence, there are subregions, where homogeneous NO and AFT phases (on the left and right side, respectively, of the PS region) are metastable (they have higher free energy than that of the PS state). For $T = 0$, the metastability boundaries coincide with the PS boundaries at $n = 0$ (the NO phase metastability) and

$n = 2/3$ (the AFT phase metastability) and they merge again at the TCP point ($k_B T = J/6$). Between the dash-dotted lines homogeneous phases are unstable.

For $U < 0$ the situation is much more complex. Although dash-dotted line marking the boundary of metastability of the AFT phase still coincides with the PS boundary at $T = 0$, this is no longer true for the NO metastability line. At $U = 0$ this boundary at $T = 0$ appears at concentration $n = 1$. For any finite and negative U , the NO is metastable at full range of concentrations at low temperatures. This applies also to the parameters outside the PS state occurrence region, where the AFT phase is a stable solution. This region expands to higher temperatures with decreasing U (Fig. 4(d)). For $U/J < -1/3 \ln 2 \approx 0.23$, the second order boundary vanishes together with the TCP. Two PS state boundaries merge at concentration $n = 1$ and the AFT metastability boundary gets its maximum also at $n = 1$, but at higher temperatures (Fig. 4(e)). For $U/J < -0.279$ the NO metastability boundary vanishes and the NO phase is (meta)stable for any n (Fig. 4(f)). For $U/J < -1/2$, the PS state does not occur any longer, but still, the AFT phase is metastable for $U/J > -1$. In such conditions, the metastable AFT phase exists in the region of the NO phase stability.

For the case of $J < 0$, the boundaries can be obtained from results presented above by using simple transformations (10)-(11). If the results for $J > 0$ are qualitatively different from these in Figs. 4, they are marked in the figure by gray dashed and dotted lines. In fact, this applies exclusively to the PS-FER boundary and the FER metastability line. Note also that the mean-field solutions of the investigated model for $n = 1$ can be mapped into the mean-field solutions of other lattice models (various extended Hubbard models in the atomic limit), see e.g., Refs. [25, 37] and references therein.

5. Conclusions and final remarks

In the present work, we investigated phase diagrams of the generalization of the Ising model on the triangular lattice. Despite the simplicity of model (1) and used approximation, the results found are not trivial. We determined the phase diagrams for both signs of magnetic interactions at the ground state (rigorous results) and for finite temperatures (the mean-field approximation). For antiferromagnetic coupling, the ordered phase (the AFT phase), where the magnetic order (with $s_A = -s_B \neq 0$ and $s_C = 0$) coexists with the charge order (non-homogeneous distribution of the particle concentration, $n_A = n_B \neq n_C$, for $n \neq 1$), occurs. This coexistence of these two orders is a consequence of the geometrical frustration of the analyzed system. In contrary, for ferromagnetic coupling, only magnetic order exists (the FER phase with $s_A = s_B = s_C$ and $n_A = n_B = n_C$), similarly as for a case of bipartite lattices. For fixed particle concentration, the phase separation state occurs away from the half-filling. Additionally, the regions for metastable phases were determined. These regions results from discontinuous transitions existing in the system.

Acknowledgements

K.J.K. thanks the Polish National Agency for Academic Exchange for funding in the frame of the Bekker programme (PPN/BEK/2020/1/00184). K.J.K. is also grateful to prof. Beata Ziaja-Motyka and Center for Free-Electron Laser Science CFEL (Deutsches Elektronen-Synchrotron DESY, Hamburg, Germany) for hospitality during a part of the work on this project.

Declaration of Competing Interest

The authors declare that they have no known competing financial interests or personal relationships that could have appeared to influence the work reported in this paper. The funders had no role in the design of the study; in the collection, analyses, or interpretation of data; in the writing of the manuscript, or in the decision to publish the results.

CRediT authorship contribution statement

Konrad Jerzy Karcia: Conceptualization, Methodology, Software, Validation, Formal analysis, Investigation, Resources, Data curation, Writing - Original draft preparation, Writing - Review & Editing, Visualization, Supervision, Project administration, Funding acquisition. **Jan Barański:** Validation, Formal analysis, Investigation, Writing - Original draft preparation, Writing - Review & Editing, Visualization.

References

- [1] R. Micnas, J. Ranninger, S. Robaszkiewicz, Superconductivity in narrow-band systems with local nonretarded attractive interactions, *Rev. Mod. Phys.* 62 (1) (1990) 113–171. doi:10.1103/RevModPhys.62.113. URL <https://doi.org/10.1103/RevModPhys.62.113>
- [2] A. Georges, G. Kotliar, W. Krauth, M. J. Rozenberg, Dynamical mean-field theory of strongly correlated fermion systems and the limit of infinite dimensions, *Rev. Mod. Phys.* 68 (1) (1996) 13–125. doi:10.1103/RevModPhys.68.13. URL <https://doi.org/10.1103/RevModPhys.68.13>
- [3] M. Imada, A. Fujimori, Y. Tokura, Metal-insulator transitions, *Rev. Mod. Phys.* 70 (4) (1998) 1039–1263. doi:10.1103/RevModPhys.70.1039. URL <https://doi.org/10.1103/RevModPhys.70.1039>
- [4] J. K. Freericks, V. Zlatić, Exact dynamical mean-field theory of the Falicov-Kimball model, *Rev. Mod. Phys.* 75 (4) (2003) 1333–1382. doi:10.1103/RevModPhys.75.1333. URL <https://doi.org/10.1103/RevModPhys.75.1333>
- [5] I. M. Georgescu, S. Ashhab, F. Nori, Quantum simulation, *Rev. Mod. Phys.* 86 (1) (2014) 153–185. doi:10.1103/RevModPhys.86.153. URL <https://doi.org/10.1103/RevModPhys.86.153>
- [6] O. Dutta, M. Gajda, P. Hauke, M. Lewenstein, D.-S. Lühmann, B. A. Malomed, T. Sowiński, J. Zakrzewski, Non-standard Hubbard models in optical lattices: a review, *Rep. Prog. Phys.* 78 (6) (2015) 066001. doi:10.1088/0034-4885/78/6/066001. URL <https://doi.org/10.1088/0034-4885/78/6/066001>
- [7] J. Struck, C. Ölschläger, R. L. Targat, P. Soltan-Panahi, A. Eckardt, M. Lewenstein, P. Windpassinger, K. Sengstock, Quantum simulation of frustrated classical magnetism in triangular optical lattices, *Science* 333 (6045) (2011) 996–999. doi:10.1126/science.1207239. URL <https://doi.org/10.1126/science.1207239>

- [8] T. Mishra, S. Greschner, L. Santos, Density-induced geometric frustration of ultra-cold bosons in optical lattices, *New J. Phys.* 18 (4) (2016) 045016. doi:10.1088/1367-2630/18/4/045016.
URL <https://doi.org/10.1088/1367-2630/18/4/045016>
- [9] K. J. Kapcia, Charge order of strongly bounded electron pairs on the triangular lattice: the zero-bandwidth limit of the extended Hubbard model with strong onsite attraction, *J. Supercond. Nov. Magn.* 32 (9) (2019) 2751–2757.
URL <https://doi.org/10.1007/s10948-019-5013-8>
- [10] K. J. Kapcia, Charge-order on the triangular lattice: A mean-field study for the lattice $S = 1/2$ fermionic gas, *Nanomaterials* 11 (5) (2021) 1181. doi:10.3390/nano11051181.
URL <https://doi.org/10.3390/nano11051181>
- [11] K. J. Kapcia, Charge-order on the triangular lattice: Effects of next-nearest-neighbor attraction in finite temperatures, *J. Magn. Magn. Mater.* 541 (2022) 168441. doi:10.1016/j.jmmm.2021.168441.
URL <https://doi.org/10.1016/j.jmmm.2021.168441>
- [12] R. M. F. Houtappel, Statistics of two - dimensional hexagonal ferromagnetics with “Ising” -interaction between nearest neighbours only, *Physica* 16 (4) (1950) 391–392. doi:10.1016/0031-8914(50)90083-8.
URL [https://doi.org/10.1016/0031-8914\(50\)90083-8](https://doi.org/10.1016/0031-8914(50)90083-8)
- [13] R. M. F. Houtappel, Order-disorder in hexagonal lattices, *Physica* 16 (5) (1950) 425–455. doi:10.1016/0031-8914(50)90130-3.
URL [https://doi.org/10.1016/0031-8914\(50\)90130-3](https://doi.org/10.1016/0031-8914(50)90130-3)
- [14] C. E. Campbell, M. Schick, Triangular lattice gas, *Phys. Rev. A* 5 (4) (1972) 1919–1925. doi:10.1103/PhysRevA.5.1919.
URL <https://doi.org/10.1103/PhysRevA.5.1919>
- [15] M. Kaburagi, J. Kanamori, Ordered structure of adatoms in the extended range lattice gas model, *Jap. J. Appl. Phys.* 13 (S2) (1974) 145–148. doi:10.7567/JJAPS.2S2.145.
URL <https://doi.org/10.7567/JJAPS.2S2.145>
- [16] B. D. Metcalf, Ground state spin orderings of the triangular Ising model with the nearest and next nearest neighbor interaction, *Phys. Lett. A* 46 (5) (1974) 325–326. doi:10.1016/0375-9601(74)90247-3.
URL [https://doi.org/10.1016/0375-9601\(74\)90247-3](https://doi.org/10.1016/0375-9601(74)90247-3)
- [17] B. Mihura, D. P. Landau, New type of multicritical behavior in a triangular lattice gas model, *Phys. Rev. Lett.* 38 (17) (1977) 977–980. doi:10.1103/PhysRevLett.38.977.
URL <https://doi.org/10.1103/PhysRevLett.38.977>
- [18] M. Kaburagi, J. Kanamori, Ground state structure of triangular lattice gas model with up to 3rd neighbor interactions, *J. Phys. Soc. Jpn.* 44 (3) (1978) 718–727. doi:10.1143/JPSJ.44.718.
URL <https://doi.org/10.1143/JPSJ.44.718>
- [19] W. Kłobus, K. Kapcia, S. Robaszkiewicz, Magnetic orderings and phase separations in the zero-bandwidth limit of the extended Hubbard model with intersite magnetic interactions, *Acta Phys. Pol. A* 118 (2) (2010) 353–355. doi:10.12693/APhysPoA.118.353.
URL <http://doi.org/10.12693/APhysPoA.118.353>
- [20] S. Murawski, K. Kapcia, G. Pawłowski, S. Robaszkiewicz, On the phase diagram of the zero-bandwidth extended Hubbard model with intersite magnetic interactions for strong on-site repulsion limit, *Acta Phys. Pol. A* 121 (5-6) (2012) 1035–1037.
URL <http://przyrbwn.icm.edu.pl/APP/ABSTR/121/a121-5-13.html>
- [21] F. Mancini, E. Plekhanov, G. Sica, $T = 0$ phase diagram of the 1D Hubbard model with magnetic interactions in the narrow band limit, *Open Physics (previously Central Eur. J. Phys.)* 10 (3) (2012) 609–614. doi:10.2478/s11534-012-0017-z.
URL <https://doi.org/10.2478/s11534-012-0017-z>
- [22] F. Mancini, E. Plekhanov, G. Sica, Exact solution of the 1D Hubbard model in the atomic limit with inter-site magnetic coupling, *Eur. Phys. J. B* 86 (5) (2013) 224. doi:10.1140/epjb/e2013-40046-y.
URL <https://doi.org/10.1140/epjb/e2013-40046-y>
- [23] S. Murawski, K. J. Kapcia, G. Pawłowski, S. Robaszkiewicz, Some properties of two-dimensional extended repulsive Hubbard model with intersite magnetic interactions – a Monte Carlo study, *Acta Phys. Pol. A* 126 (4-A) (2014) A–110–A–113.
URL <http://doi.org/10.12693/APhysPoA.126.A-110>
- [24] S. Murawski, K. J. Kapcia, G. Pawłowski, S. Robaszkiewicz, Monte Carlo study of phase separation in magnetic insulators, *Acta Phys. Pol. A* 127 (2) (2015) 281–283.
URL <http://doi.org/10.12693/APhysPoA.127.281>
- [25] K. J. Kapcia, S. Murawski, W. Kłobus, S. Robaszkiewicz, Magnetic orderings and phase separations in a simple model of insulating systems, *Physica A* 437 (2015) 218–234. doi:10.1016/j.physa.2015.05.074.
URL <https://doi.org/10.1016/j.physa.2015.05.074>
- [26] S. Murawski, G. Musiał, G. Pawłowski, Parallel Monte Carlo simulations for spin models with distributed lattice, in: R. Wyrzykowski, E. Deelman, J. Dongarra, K. Karczewski, J. Kitowski, K. Wiatr (Eds.), *Parallel Processing and Applied Mathematics*, Springer International Publishing, Cham, 2016, pp. 332–341. doi:10.1007/978-3-319-32152-3_31.
URL https://doi.org/10.1007/978-3-319-32152-3_31
- [27] K. J. Kapcia, W. Kłobus, S. Robaszkiewicz, Some exact results for the zero-bandwidth extended Hubbard model with intersite charge and magnetic interactions, *Acta Phys. Pol. A* 127 (2) (2015) 284–286.
URL <http://doi.org/10.12693/APhysPoA.127.284>
- [28] S. Robaszkiewicz, Magnetism and charge-ordering in localized state, *Phys. Status Solidi B - Basic Research* 70 (1) (1975) K51–K54. doi:10.1002/pssb.2220700156.
URL <https://doi.org/10.1002/pssb.2220700156>
- [29] S. Robaszkiewicz, Magnetism and charge orderings in Mott insulators, *Acta Phys. Pol. A* 55 (4) (1979) 453–469.
- [30] R. Micnas, S. Robaszkiewicz, K. A. Chao, Multicritical behavior of the extended Hubbard model in the zero-bandwidth limit, *Phys. Rev. B* 29 (5) (1984) 2784–2789. doi:10.1103/PhysRevB.29.2784.
URL <https://doi.org/10.1103/PhysRevB.29.2784>
- [31] J. Jędrzejewski, Electron charge ordering in the extended Hubbard model, *Z. Phys. B - Condens. Matter* 48 (3) (1982) 219–225. doi:10.1007/BF01420583.
URL <http://doi.org/10.1007/BF01420583>
- [32] J. Jędrzejewski, On the phase diagram of the extended Hubbard model, *Z. Phys. B - Condens. Matter* 59 (3) (1985) 325–332. doi:10.1007/BF01307438.
URL <http://doi.org/10.1007/BF01307438>
- [33] U. Brandt, J. Stolze, Ground states of extended Hubbard models in the atomic limit, *Z. Phys. B - Condens. Matter* 62 (4) (1986) 433–441. doi:10.1007/BF01303574.
URL <http://doi.org/10.1007/BF01303574>
- [34] J. Jędrzejewski, Phase diagrams of extended Hubbard models in the atomic limit, *Physica A* 205 (4) (1994) 702–717. doi:10.1016/0378-4371(94)90231-3.
URL [https://doi.org/10.1016/0378-4371\(94\)90231-3](https://doi.org/10.1016/0378-4371(94)90231-3)
- [35] C. Borgs, J. Jędrzejewski, R. Kotecký, The staggered charge-order phase of the extended Hubbard model in the atomic limit, *J. Phys. A: Math. Gen.* 29 (4) (1996) 733–747. doi:10.1088/0305-4470/29/4/005.
URL <http://doi.org/10.1088/0305-4470/29/4/005>
- [36] K. J. Kapcia, J. Barański, A. Ptok, Diversity of charge orderings in correlated systems, *Phys. Rev. E* 96 (4) (2017) 042104. doi:10.1103/PhysRevE.96.042104.
URL <https://doi.org/10.1103/PhysRevE.96.042104>
- [37] K. Kapcia, Metastability and phase separation in a simple model of a superconductor with extremely short coherence length, *J. Supercond. Nov. Magn.* 27 (4) (2014) 913–917. doi:10.1007/s10948-013-2409-8.
URL <http://doi.org/10.1007/s10948-013-2409-8>
- [38] E. Arrigoni, G. C. Strinati, Doping-induced incommensurate antiferromagnetism in a Mott-Hubbard insulator, *Phys. Rev. B* 44 (14) (1991) 7455–7465. doi:10.1103/PhysRevB.44.7455.
URL <https://doi.org/10.1103/PhysRevB.44.7455>
- [39] M. Bąk, Mixed phase and bound states in the phase diagram of the extended Hubbard model, *Acta Physica Polonica A* 106 (5) (2004) 637–646. doi:10.12693/APhysPoA.106.637.
URL <http://doi.org/10.12693/APhysPoA.106.637>